

1 **Structural Collapse in Kaolinite, Montmorillonite and Illite Clays by**
2 **Infrared Spectroscopy and its Role in Ceramic Rehydroxylation Dating**
3 **of Low-Fired Earthenware**

4
5 Christopher M. Stevenson*, Anthropology Program, School of World Studies, Virginia
6 Commonwealth University, Richmond, Virginia

7
8 Mary Gurnick, Department of Science and Quantitative Methods, Richard Bland College,
9 The College of William and Mary, Petersburg, Virginia

10
11 *Corresponding author: Ph: 804-827-2418/Fax: 804-827-3479

12 e-mail: cmstevenson@vcu.edu

13
14
15 **Abstract**

16
17 *The rehydroxylation dating of ancient pottery estimates the age of ceramic manufacture*
18 *based upon the total hydroxyl (OH) accumulation since initial firing. The diffusion of*
19 *OH is impacted by the structural porosity of the ceramic that becomes progressively, or*
20 *suddenly, closed with increasing temperature as the clay structure collapses. Changes in*
21 *ceramic mineral structure along the temperature continuum occur at certain thermal set*
22 *points. Infrared spectroscopic analysis of thermally treated kaolin, illite, and*
23 *montmorillonite reveals that shifts in the Si-O band correlate with the extent of structural*

24 *collapse occurring between 600-1000°C and the degree of structural collapse in*
25 *prehistoric earthenware ceramics may be estimated using this approach. Accelerated*
26 *rehydroxylation experiments reveal that the activation energy of rehydroxylation*
27 *decreases with greater structural collapse and indicates that the rate of rehydroxylation*
28 *will be faster for ceramics fired at more elevated temperatures.*

29

30 Keywords: clay, infrared, firing temperature, rehydroxylation, dating, ceramic

31

32 **1. Introduction**

33

34 The ceramic rehydroxylation (RHX) dating of bricks, terracotta tiles and
35 archaeological pottery (Tosheva et al. 2010; Wilson et al. 2009, 2012, 2014) has captured
36 the interest of archaeologists who work diligently at developing and refining
37 chronological sequences using ceramic materials from archaeological contexts.
38 Chronology building is especially challenging in locations where earthenware, with
39 modest amounts of surface decoration, are part of the cultural assemblage. Any number
40 of regions in the world can be used as an example whether it is the Woodland Period of
41 the Southeastern United States (Smith and Neiman 2007) or the prehistoric ceramic
42 sequence of Fiji (Sand et al. 2000). In such contexts, chronological sequences may be
43 categorized simply as early, middle and or late, and constitute periods spanning 200-500+
44 years. On a larger regional basis, it is difficult to correlate multiple local chronologies or
45 to trace evolving historical ceramic traditions with such large temporal periods. Put

46 simply, the poor temporal resolution restricts the ability to evaluate hypotheses about past
47 behavior and to easily engage in the emerging social archaeology of the present.

48

49 Ceramic rehydroxylation dating is a self-calibrating method that provides a rate
50 constant for hydroxyl (OH) diffusion intrinsic to the sample under study. It generates an
51 age assessment for the last heating, or dehydroxylation (DHX), event. This may reflect
52 initial firing, a cooking event, or the disposal and burning of pottery sherds with other
53 domestic refuse. As such, the method has the potential to provide absolute dates for
54 individual contexts and to enhance regional chronological sequences. A recent series of
55 papers have sought to refine the initial rehydroxylation model of Wilson et al. (2009) by
56 the examination of central issues such as environmental temperature estimation (Hall et
57 al. 2013), the impacts of mass gain during cooling (Barrett 2013), and the impacts of
58 humidity (Bowen et al. 2011; Drelich et al. 2013). In this study, we look at another key
59 aspect of the dating method; that of structural changes in the clay matrix induced during
60 firing and the impact it has on the rehydroxylation process.

61

62 **2. Background to Ceramic Rehydroxylation Dating**

63

64 As originally described by Wilson et al. (2009) the DHX/RHX process was
65 discussed for kaolin, montmorillonite, and chlorite clays. During the ceramic
66 manufacturing process raw clay may be fired within kilns at temperatures up to
67 approximately 1200°C. As the temperature is raised above ambient conditions,
68 physically adsorbed water is lost just above 100°C. Between 105°C and 500°C

69 chemisorbed water, or bonded H₂O, is removed from the interlayers and surfaces of any
70 mineral features (Drits and McCarthy 2007). At 500-900°C hydroxyl is removed as the
71 dehydroxylation of bonded water takes place ($2\text{OH}^- \rightarrow \text{H}_2\text{O} + \text{O}^{2-}$). The temperature at
72 which DHX initiates is dependent upon the structure of the clay matrix. The removal of
73 water is likely a complex reaction that may include both diffusion and first-order kinetics
74 (Ortega et al. 2010).

75
76 Once a ceramic is removed from the kiln and allowed to cool, rehydroxylation
77 begins immediately and occurs in two stages. Initially, there is a rapid gain in mass as
78 molecular water and hydroxyl is adsorbed onto the surface and into the pore structure of
79 the ceramic (Stage 1). This process decreases with time and is replaced by a $t^{0.25}$ gain
80 (Wilson et al. 2003; Wilson et al. 2009; Hall et al. 2013; Hamilton and Hall 2012) in
81 mass as a result of hydroxyl migration through the boundary layers between the ceramic
82 microcrystalline particles (Stage 2). The exact mechanism of this process is not known
83 but is assumed to be a single-file type of solid state transport. This would account for the
84 slow inward movement of water over time. In laboratory mass gain experiments, the
85 amount of available molecular water is arbitrarily restricted (Savage et al. 2008; Wilson
86 et al. 2014) during RHX by exposing the ceramic to a low relative humidity (e.g., 30-
87 35%) that inhibits the adsorption of excess surface water and allows the mass uptake of
88 OH to be tracked. In archaeological contexts additional water may accumulate in the
89 larger pore structure from rain but the excess water does not accelerate the RHX process
90 (Wilson et al. 2009).

91

92 Encouraging dating results have emerged from the application of the RHX dating
93 method (Wilson et al. 2009). Follow-up investigations after the initial study have
94 identified significant deviations from the outlined protocols. Several investigations
95 (Bowen et al. 2013; Le Goff and Gallet 2015) have argued that the $t^{0.25}$ power law that
96 defines the RHX rate is not always observed and that a variable exponent (t^n) is needed to
97 account for variation in the experimental data. In addition, others note that scrutiny of the
98 completeness of sample drying and dehydroxylation (Le Goff and Gallet 2014) and the
99 effect of contaminating carbon (Numrich et al. 2015) are needed.

100

101 In contrast to advanced ceramic production, prehistoric earthenware was
102 hardened through open firing within pits, or on the ground surface, where the surrounding
103 fuel of wood, or dung, generated temperatures that were several hundred degrees lower
104 than kiln environments. Ethnographic and experimental data indicate that firing
105 temperatures may range between 300-900°C (Shepard 1976; Gosselain 1992). In
106 addition, the thermal gradients associated with open firing can be highly variable
107 depending upon the fuel load, number of pots, and their physical separation. Careful
108 monitoring with thermocouples revealed that temperature variation within a firing event
109 may range up to 390°C (Maggetti et al. 2011). Under such circumstances, and with many
110 observed firing durations under two hours (Smith 2001), the clay vessels have the
111 potential not be full dehydroxylated, and variable in terms of clay crystalline structure.

112

113 This variability in clay structural states has the potential to impact the rate of
114 rehydroxylation for low fired ceramics. While the self-calibrating nature of the dating

115 process compensates for this situation by developing a hydroxyl diffusion coefficient
116 specific to the material state, it is informative to explore the impact of structural collapse
117 on hydroxyl diffusion, since future research may explore the development of a predictive
118 model of RHX based upon ceramic molecular structure. Thus, we look at the
119 dehydroxylation of kaolinite, montmorillonite and illite to determine at what
120 temperatures critical structural changes occur and how we can identify these temperatures
121 in archaeological materials using infrared spectroscopic analysis. We then show how
122 these structural changes impact the subsequent OH diffusion process as reflected by the
123 changes in activation energy of RHX.

124

125 **3. Dehydroxylation and Structural Change in Kaolinite, Montmorillonite, and Illite**

126

127 Kaolinite, montmorillonite, and illite were some of the most common minerals
128 used in the manufacture of prehistoric ceramics, and as such, understanding structural and
129 mineralogical changes during heating is central to the process. The thermal treatment of
130 clay has been extensively investigated and reveals how the mechanisms of water loss
131 vary between kaolinite, montmorillonite, and illite. We summarize this previous research
132 to identify changes in ceramic molecular structure with temperature and hypothesize how
133 this might impact the RHX process.

134

135 *Kaolinite*

136

137 Kaolinite, a dioctahedral 1:1 clay, with the formula $\text{Al}_2\text{Si}_2\text{O}_5(\text{OH})_4$ and its
138 dehydroxylation has been thoroughly studied with a variety of analytical techniques
139 including scanning electron microscopy [SEM] (Felicissimo et al. 2010), X-ray
140 diffraction [XRD] (Marghussian et al. 2009) and Fourier transform infrared spectroscopy
141 [FTIR] (Frost 1996). This type of clay is known to be an inorganic polymer with a two-
142 dimensional layered structure (Frost et al. 2003). In each layer, a sheet of SiO_2 tetrahedra
143 is bonded at the apices of the tetrahedral to a sheet of aluminum (III) octahedra with four
144 of the six octahedral sites occupied by hydroxyl groups. Two of every three aluminum
145 octahedral sites are occupied resulting in lattice distortion which lowers the crystal
146 symmetry. A direct result of the low symmetry is the rich FTIR spectrum of kaolinite.
147 The intra-layer of the hydroxyls is located in the same plane as the apical oxygen, while
148 the remaining three hydroxyls are directed toward the interlayer space and hydrogen bond
149 with the silica of the adjoining layer. This accounts for the lack of water in the interlayer
150 space.

151

152 After the loss of physically absorbed water between 100-200°C, the hydroxyl
153 from the inner and inner-surface migrates to the surface and dehydroxylates
154 endothermically at temperatures between 450-600°C (Zemenova et al. 2014): This
155 temperature range applies to both ordered and disordered kaolinites (Bellotto et al. 1995).
156 Beginning in this temperature range there is a structural reorganization during DHX
157 where metakaolin is formed. A progressive distortion and collapse of the clay 1:1
158 structure occurs as OH is removed and the metakaolin nucleates. At this point the
159 interlaminar channels that allow water to be removed are blocked (Ortega et al. 2010;

160 Sperinek et al. 2011). This results in some residual OH remaining in the ceramic. The
161 metakaolin becomes progressively a less layered structure as temperature increases.

162

163 The next phase transformation occurs at about 950°C when spinel is formed.
164 This is followed by a transformation to mullite between 950-1100°C. At the end of this
165 process a nearly water free, highly vitrified ceramic is produced. For ceramics fired at
166 temperatures below 950°C, we can conceive of the kaolin molecular structure as a
167 continuum exhibiting varying degrees of deformation and channel blockage (Pesova et al.
168 2010).

169

170 *Montmorillonite*

171

172 Montmorillonites are a type of 2:1 dioctahedral phyllosilicates with the general
173 formula: $(Al_{(2-y)}Mg_y)(Si_{(4-x)}Al_x)O_{10}(OH)_2M_{(x+y)}.nH_2O$, where $y > x$ an M represents
174 interlayer exchangeable cations. These clays are somewhat turbostratic (Viani et al.
175 2002), swellable, and have substantial capacity to exchange interlayer cations. Individual
176 clay layers consist of two sheets of tetrahedral silica covalently bonded through apical
177 oxygen to a middle sheet of aluminous octahedra. The bases of the silica tetrahedra form
178 hexagonal cavities, which face the interlayer space. One, out of every three, octahedral
179 sites is vacant. Hydroxyl group pairs can be located either cis- or trans-coordinated to the
180 cation in the octahedral layer (Drits et al. 1995; Tshipursky and Drits 1984). Two thirds
181 of the middle octahedra contain a metal ion, most commonly trivalent aluminum, but
182 frequently divalent ions like magnesium, which give the middle octahedral sheet an
183 overall negative charge. The charge is balanced through long-range interactions with

184 cations in the interlayer space.

185

186 Normally these exchangeable ions in the interlayer are hydrated. The interlayer
187 space can contain one to three layers of water molecules. The hydration of smectites
188 have been well studied (Grim and Bradley 1948; Muller et al. 2002) and is known to
189 depend on several factors including the type of interlayer cation, amount of layer charge
190 (Sato et al. 1992) and environmental factors like humidity (Ferrage et al. 2005), external
191 vapor pressure and temperature. At normal pressures montmorillonites dehydrate losing
192 interlayer water between 120°C and 200°C (Bala et al. 2000).

193

194 Montmorillonites dehydroxylate when a proton moves from one hydroxyl to an
195 adjacent hydroxyl to form a water molecule and aluminum cations coordinate to the
196 remaining oxygen. Trans-vacant montmorillonites dehydroxylate at temperatures around
197 500-550°C to form five coordinate aluminum cations. The dehydroxylation temperature
198 of cis-vacant montmorillonites is higher, around 700°C. An unstable mixture of five and
199 six coordinate octahedral forms and as a result aluminum cations migrate during the
200 dehydroxylation and the rehydroxylated montmorillonite will be trans-vacant (Drits et al.
201 1995). Over 900°C montmorillonites form various firing products. The actual firing
202 products and firing temperatures depend on the structure of the montmorillonite. Most
203 montmorillonites form a spinel over 1000°C. Other firing products may include B
204 quartz, anorthite, enstatite, mullite and cristabolite (Bradley and Grim 1951).

205

206 *Illite*

207

208 Illite has the nominal formula $(K_{0.88} Al_2(Si_{3.12} Al_{0.88})O_{10} (OH)_2$. It is a non-
209 expanding 2:1 clay that is constructed from two tetrahedral sheets that sandwich a central
210 octrahedral sheet. The interlayer of K, Na, Ca, and Ba serve to inhibit the presence of
211 water molecules and prevent swelling except for K-deficient varieties which may allow
212 water into the interlayer region (Yates and Rosenberg 1997). The dehydroxylation and
213 phase transformations for illite are also well known. DHX begins with the condensation
214 of water molecules in the octahedral layer and results from Al-O bond breaking. This is
215 followed by a one-dimensional diffusion of water molecules through the tetrahedral ring
216 into the interlayer region that can occur at between 350-675°C (McConville and Lee
217 2005). The crystalline structure is still in place until 700°C but then begins to break
218 down between 700-850°C. Above this temperature there is a second endothermic
219 dehydroxylation. In K-deficient illites water molecules then make their way through the
220 interlayer region along two-dimensional pathways that are directed by K^+ ion vacancies.
221 This latter diffusion occurs between 875-1100°C (Gualtiere and Ferrari 2006). Also
222 above 800°C the octahedral sheet crystallizes a spinel which grows in crystal size and
223 then melts at 1300°C. Mullite crystals begin to form at 1100°C and melt above 1400°C.

224

225 In summary, kaolinite begins to dehydroxylate at 450-600°C and progressively
226 loses hydroxyl until a complete conversion to metakaolinite at 950-1100°C. Trans-vacant
227 montmorillonites dehydroxylate rapidly at 500-550°C and cis-vacant forms lose hydroxyl
228 at 700°C. Similarly, illites, other than K-deficient forms, also lose hydroxyl rapidly at
229 700-850°C while the K-deficient forms dehydroxylate at a higher temperature range of

230 875-1100°C. Based upon these observations, we hypothesize that the gradual structural
231 collapse of kaolinite will incrementally block the OH diffusion pathways during RHX
232 and the rate of RHX should gradually decrease with higher firing temperatures. For illite
233 and montmorillonite, the more temporally restricted periods of structural collapse should
234 result in a substantial change in the rate of OH diffusion after the rapid structural collapse
235 event. Our ability to monitor the degree of structural collapse for experimental or
236 prehistoric ceramics depends upon establishing the thermal history of the sample.

237

238 **4. Estimation of Firing Temperature by Infrared Transmission Spectroscopy**

239

240 The estimation of ceramic firing temperature has been used in a number of studies
241 focused on the reconstruction of ceramic technology during manufacture (Cultrone et al.
242 2001; Mirti et al. 2006; Shoval and Beck 2005; Papadopoulou et al. 2006; Drebuschchak
243 et al. 2007; Krapukaityte et al. 2008; Trindale et al. 2009; Wolf 2002). Estimating this
244 parameter generally relies upon changes in the mineral composition, as determined by X-
245 ray diffraction of the ceramic, as temperature increases. These changes may include the
246 breakdown and disappearance of minerals, the crystallization of minerals, and the
247 appearance of new mineral phases. Charts of progressively changing mineral associations
248 developed from experimental firings guides the researcher in estimating a firing
249 temperature usually to within a 100-200°C range for the archaeological sample. In
250 addition, there are other approaches that may involve the use of electron paramagnetic
251 resonance (EPR) to follow spectral changes in Fe^{3+} or Mn^{2+} with temperature
252 (Felicissimo et al. 2010) or Mossbauer spectroscopy to track the oxidation states of iron

253 oxides (Venkatachalapathy et al. 2002; Wagner et al. 1999). Investigations such as this
254 may jointly use scanning electron microscopy (SEM) to examine matrix structural
255 changes or X-ray diffraction (XRD) to document different mineral phases occurring
256 before and after firing (Mirti and Davit 2001; Venkatachalapathy et al. 2008). These
257 methods result in the estimation of temperature minima or broad temperature ranges.
258

259 A more frequently used tool is that of Fourier transform infrared spectroscopy
260 (FTIR) often in conjunction with some of the complementary analytical techniques
261 mentioned above (Shoval 2003; Odriozola and Martinez-Blanes 2007; Palanivel and
262 Rajesh Kumar 2011). In this approach, changes in the infrared spectra such as peak
263 minimization or disappearance, peak shape deformation, and peak wavenumber position
264 are tracked at unique firing intervals usually within the range of 400-1200°C. In
265 conjunction with XRD, and the identification of mineral peaks on the infrared spectra
266 (Benedetto et al. 2002), upper and lower firing limits that have a range of 50-200°C may
267 be established (Tite 1999). However, until recently none of the infrared based
268 investigations have researchers identified a mineral or hydroxyl band that shifts
269 continuously as a function of increasing temperature. In an early work, Shoval (2003)
270 came closest to this goal where he notes significant shifts in the Si-OH stretching band
271 and Al-OH/Si-OH deformation bands in ancient calcareous ceramics but these trends are
272 not quantified and numerically described in the form of a prediction equation. More
273 recently, he identified a linear increase in the SiO stretching band to higher wavenumbers
274 between 500-900°C for kaolinite and a more abrupt upward shift for smectite (Shoval et
275 al. 2011).

276

277 In this study, we use FTIR spectroscopy to identify predictable shifts in the Si-O
278 infrared peaks for the refined kaolin, montmorillonite, and illite clays fired between 600-
279 1000°C. Gradual and abrupt transformations in the clay structure are identified as a
280 function of temperature. These results are compared to the process of structural collapse
281 in three naturally occurring clays from St. Catherine’s Island, Georgia, and the structural
282 states of a small sample of six prehistoric earthenware ceramics are examined to assess
283 the range of firing temperatures, since the latter materials will eventually be dated by
284 RHX and compared with independent radiocarbon chronometric data.

285

286

287 **5.0 Analytical Methods**

288

289 The refined source clays used in this analysis consisted of a high-defect kaolinite
290 (KGa-2) and montmorillonite (STx-1b) from the Clay Minerals Society of Virginia and
291 an illite from Wards Natural Science (Green Shale 46E0315). These clay types were
292 selected since prehistoric earthenware may contain one or more of these materials. These
293 clays have been thoroughly characterized and compositional analysis of the kaolinite and
294 montmorillonite is documented by Mermut and Cano (2001). The illite consists of shale
295 containing illite (85%) and quartz obtained in the vicinity of Rochester, New York.
296 Compositional information on this material has been published by Cloutis (2001).

297

298 Our eventual goal of dating ceramics from prehistoric sites on St. Catherine's
299 Island, Georgia, prompted us to assess the clay sources that might have been used by
300 potters prior to European, and during, contact in the 17th century. Samples of three clays
301 identified during the island survey were obtained through shallow hand excavations.
302 These materials originated from the South End Field (SCI-RC-1), South Beach (SCI-RC-
303 2), and North Beach (SCI-RC-4) of the island (Figure 1). Their location within 2-7
304 kilometers of the Santa Catalina Mission and prehistoric sites on the island suggested
305 they might have been used in the ceramic manufacturing process. X-ray diffraction was
306 completed on one sample from each of the raw clays to provide a preliminary, yet not
307 fully representative, assessment their mineral structure in this exploratory study. The
308 clays were ground with an agate mortar and pestle and passed through a 43 μ m sieve. An
309 Expert-Pro Pan Analytical diffractometer system scanned the powders between the 5.01-
310 79.97 °2-Theta positions with a step size of 0.0260. Mineral contributions to the clay
311 were identified based upon the position and intensity of 2-Theta intensity values using
312 published data bases (e.g., Bish 2010; Drits et al. 2010; Viani et al. 2002).

313

314 The ceramic heating experiments were conducted in a Thermolyne muffle furnace
315 between 600°C and 1000°C at 100 degree intervals for both the refined and raw clays.
316 Small porcelain crucibles held 0.1 gram of powdered clay for each exposure. The extent
317 of dehydroxylation is related to the time the material spends in the kiln (Criado et al.
318 1984). Biljana et al. (2010) found dehydroxylation of kaolinite to be complete after 60-
319 90 minutes. Ogloza and Malholtra et al. (1989) suggest a 24-hour residence time for
320 montmorillonite. In our experiments the clays of kaolinite, montmorillonite and illite

321 experienced a residence time of 24 hours (Table 1). The clays from St. Catherine's
322 Island heated from 600-700°C remained at the set temperature for 24 hours, while
323 samples at the higher temperatures of 800-1000°C were left in the oven for 3-4 hours
324 (Table 2).

325

326 Infrared analysis of the thermally altered clays was conducted by transmission of
327 sample material contained within KBr pellets. A Thermo Nicolet Avatar 360 FTIR with
328 a DTGS detector and KBr beamsplitter was used to collect spectra covering the
329 wavelength region between 4000-400cm⁻¹. Each spectrum consisted of 64 averaged
330 scans collected at a resolution of 4cm⁻¹ and a mirror velocity of 0.4747cm/s. The samples
331 were prepared using 200mg of dried KBr powder mixed with 2 mg of sample. A pressed
332 pellet was then prepared on a Spex 3628 bench-press under 10 tons of pressure. Single
333 samples were heated at each temperature to illustrate general trends in clay structural
334 collapse in this preliminary evaluation.

335

336 The estimation of firing temperatures on a sample of prehistoric ceramics also
337 utilized the same infrared analytical procedures. Six sherds were selected from Late
338 Mississippian/Mission Period (ca. AD1500-1700) contexts at sites 9Li8 and 9Li207.
339 Sherd 4079 (9Li207) was a 1cm thick wide fragment and 2mg subsamples were taken
340 from across its profile to evaluate the variation in thermal history. The remaining five
341 sherds (9Li8) were 4-5mm wide and samples were extracted from well oxidized sections
342 using a steel blade.

343

344 Ceramic activation energies for the refined clays were determined by the
345 measurement of diffused hydroxyl by infrared diffuse reflectance. Each activation
346 energy was based on the measurement of five diffusion coefficients empirically
347 determined by RHX of clay samples reacted between 600°C and 900°C at 100 degree
348 intervals. A Pike Technologies Diffuse-IR temperature controlled reaction chamber
349 mounted in the compartment of a Perkin Elmer Frontier infrared spectrometer was used
350 to control the environment around the sample. Fine powders of kaolin (as recieved),
351 montmorilonite ($\leq 43\mu\text{m}$), and illite ($\leq 43\mu\text{m}$) constituted the starting material. Diffuse
352 reflectance spectroscopy is a technique that must be used and a uniformity of particle size
353 and compaction are essential to generate reproducible data.

354

355 The sample powder was placed within a 3mm diameter porcelain sample cup,
356 and packed to a uniform sample depth below the cup rim using the supplied tamper. The
357 cup was placed within the heating element of the reaction chamber and sealed with a lid
358 containing a ZnSe window. Infrared spectra were then programmed to be taken every 20
359 minutes for the life of the experiment using Temp-pro software. Individual spectra were
360 an average of 40 scans taken between 4000-400 cm^{-1} at a resolution of 8 cm^{-1} and a mirror
361 velocity of 0.5 cm/s . The reference spectrum was taken on a mirror immediately prior to
362 the experiment start-up.

363

364 For each experimental run the sample was dried under nitrogen at 200°C for one
365 hour. This was followed by a heating of the powder to a predefined temperature between
366 600°C - 900°C for a period of three hours under a nitrogen stream to dehydroxylate the

367 clay. The sample was then cooled to the RHX temperature and an infrared background
368 measurement was taken to remove any absorption signal from the sample cup or
369 dehydroxylated clay. The chamber purge was then switched to a humid air stream set to a
370 relative humidity of 50% at room temperature (Forney and Brandl 1992). However, the
371 elevated temperatures within the reaction chamber would reduce the relative humidity to
372 between 3-6% (Vaisala 2012) thereby requiring a longer time for the Phase 1 portion of
373 the RHX to reach completion. This duration was approximately 6.5 minutes at $t^{0.25}$
374 (Figure 7). The RHX time was set to 9000 minutes and infrared spectra were collected at
375 20 minute intervals. The amount of diffused water was determined by calculating the
376 peak area of the combination OH/H₂O water band at 3570cm⁻¹. Excel software was used
377 to plot the water absorption curve and provide best fit trend lines and slopes of the data.

378

379 **6.0 Results**

380

381 *6.1 Identification of Structural Change in Refined Clays*

382 Kaolinite (KGa-2)

383 As kaolinite (KGa-2) is fired at temperatures between 600°C and 1000°C the peak
384 position attributed to Si-O stretching frequency gradually shifts from 1075cm⁻¹ to
385 1100cm⁻¹ (Table 1). Similarly, there is a steady shift to higher wavenumbers in the peak
386 near 1200cm⁻¹ (Figure 2a). These changes likely indicate the formation of amorphous
387 silica as the metakaolinite converts to mullite.

388 Montmorillonite (STx-1b)

389 The Texas montmorillonite (STx-1b) shows a very different trend. The Si-O
390 stretching band location is steady between 600°C and 700°C at around 1042cm⁻¹ but then
391 jumps abruptly to 1090cm⁻¹ at 800°C and remains very close to this location up to 1000°C
392 (Figure 2b). The Si-O-Si deformation peak at 480cm⁻¹ (Madejova and Komadel 2001)
393 remains essentially the same during early heating and is within the resolution of the
394 instrument (4cm⁻¹). Afterward, it drops to 474cm⁻¹ by 1000°C (Table 1).

395 Illite

396 Changes in band position for illite parallel that of montmorillonite (Table 1). The
397 Si-O stretch found at 1012cm⁻¹ for 600°C shifts dramatically to 1078cm⁻¹ at 900°C-
398 1000°C. The Si-O-Si band at 482cm⁻¹ also remains stable until 900°C and then drops to
399 463cm⁻¹ indicating a structural change in the clay (Figure 2c).

400 *6.2 Analysis of Structural Changes in Raw Clays*

401 The XRD analysis revealed that the sediment samples from St. Catherine's Island
402 are a mixture of clay types. Montmorillonite is expressed by a single peak at 6.04. Illite
403 is revealed by peaks at 8.99, 19.8, 25.68, and 35.08. Kaolinite is also present and
404 expressed by peaks at 12.39, 20.95, 25.04, and 38.44. The other dominant material is
405 quartz represented by numerous peaks throughout the sequence. Samples SCI-RC-2 and
406 SCI-RC-4 contain only kaolinite and illite while sample SCI-RC-1 contains all three clay
407 types.

408 The infrared analysis of the heated clay samples from St. Catherine's Island show
409 a consistent shift in the Si-O peak location to higher wavenumbers (Figure 3, Figure 4).

410 From 500-800°C the peak position remains stable within a range of 1031-1037cm⁻¹ but
411 then abruptly shifts to 1089—1095cm⁻¹ at a temperature of 800°C and remains within this
412 range at 900°C (Table 2).

413 *6.3 Firing Temperature of Prehistoric Earthenware*

414 The infrared analysis of five sub-samples from a 1 cm wide cross-section of a
415 prehistorically fired ceramic fragment from St. Catherine's Island reveals the firing
416 history of this item. The fragment (Sherd 4079) was excavated from a prehistoric
417 habitation site (9Li207) and is most probably a locally manufactured ceramic. Sub-
418 samples were extracted from the blackened interior and across the matrix to the patterned
419 exterior surface. In each case the infrared Si-O infrared band falls between 1034-
420 1054cm⁻¹ (Figure 5), indicating that the original pot was fired at temperatures less than
421 900°C (Table 3). The additional analysis of five Late Mississippian/Woodland sherds
422 from site 9Li8 (Table 3) also have infrared peak positions located below 1090cm⁻¹,
423 indicating that the prehistoric firing did not reach 900°C.

424 *6.4 Activation Energy Determinations*

425 The activation energy (E) for each of the three refined clays were computed from
426 the experimental data of rehydroxylation collected by diffuse reflectance on five samples
427 rehydroxylated between 110°C to 150°C from each of the three refined clays
428 dehydroxylated between 600-900°C. The natural logarithm (ln) of each slope (Figure 6)
429 was regressed against the reciprocal of the reaction temperature (1/Kelvin) [Table 4].
430 The slope of the best fit line was multiplied by the universal gas constant (8.315) and the
431 product then raised to the fourth power, and multiplied by a thousand to provide an E

432 value in J/mol (Table 5).

433 The activation for kaolinite progressively declined with increasing firing
434 temperature. At 600°C the E value was 119, 218 J/mol and by 900°C it was reduced to
435 65,242 J/mol. Similarly, the starting activation energy for illite was 107,571 J/mol at
436 700°C and reduced to a lower value of 47,181 J/mol by 900°C. Montmorillonite followed
437 the same trend with an E value of 120,468 J/mol at 700°C and a value of 96,059 J/mol at
438 900°C.

439 **6.0 Discussion**

440 Our heating experiments on kaolinite, montmorillonite and illite clays document a
441 structural collapse of the crystalline structure that is registered by a shift in the main
442 infrared Si-O peak position to higher wavenumbers. This shift is gradual in kaolinite as
443 the proportion of metakaolinite increases with higher temperature. For the other two
444 clays the structural collapse is much more abrupt and the transition occurs between 700-
445 800°C in montmorillonite and between 800-900°C in illite. This rapid collapse is also
446 reflected in the unrefined clay samples from St. Catherine's Island that contain either a
447 mixture of all three clays or a combination of kaolinite and illite. In each case there is a
448 collapse of the clay structure between 800-900°C and the Si-O peak position increases by
449 about fifty wavenumbers. Even though kaolinite was present in each of the raw clays its
450 influence is not clear and is masked by the more radical shifts in peak position
451 experienced by montmorillonite and/or illite.

452 Prehistoric potters involved in the production of earthenware ceramics often used
453 open-ground firing to transform raw clay into finished ceramics. The lower (<1000°C)

454 and variable temperatures inherent to this technology, compared to that of kiln firing,
455 may produce a range of dehydroxylation states depending upon the intensity of heat
456 exposure. Our infrared analysis of six prehistoric sherds from St. Catherine's Island
457 indicates that ceramics were produced at temperatures below 900°C. Thus, the clays
458 within the sherds may not be completely dehydroxylated and the crystalline structure of
459 the clay that constitutes the ceramic body may be partially intact.

460 The presence of clay particles in different stages of dehydroxylation and structural
461 collapse has implications for the ceramic rehydroxylation dating method. The presence
462 of residual OH would not appear in itself impact the gain calculations for hydroxyl since
463 the dehydroxylation of the prehistoric sherd subject to dating removes only the
464 accumulated water gained after initial firing and does not cause any further structural
465 changes. The low temperature of dehydroxylation (500-550°C) does not remove the
466 hydroxyl that may remain attached to the preserved crystalline lattice. This can only be
467 removed by additional heating to 800°C or higher. The dehydroxylation of the ceramic
468 prior to ceramic dating serves to re-establish the state of the ceramic at the point of
469 manufacture.

470 On the otherhand the presence of both intact crystalline material and structurally
471 collapsed clay could impact the movement of OH into the ceramic. As a result of this
472 variation in matrix states, a range of diffusion coefficients can be anticipated for an
473 archaeological assemblage. Contrary to our initial hypothesis where we thought that a
474 collapsed crystalline structure would block OH diffusion, we see that the activation
475 energy of RHX is higher for underfired clays. Thus, the diffusion coefficient will be
476 smaller compared to ceramics fired at temperatures closer to 1000°C. Activation energy

477 determinations on bricks and ceramics reported by Clelland et al. (2014) range between
478 57,000 J/mol and 119,000 J/mol and these converge with the range of values reported for
479 our refined clays. Interestingly enough, activation energies on three subsamples from a
480 single sherd vary by almost 20,000 J/mol, a factor that she attributes to different thermal
481 histories even at this small scale. A similar conclusion was reached by Le Goff and Gallet
482 (2014) who attribute variation in the rate of RHX on ancient Syrian ceramics to variable
483 activation energies for sherds from the same archaeological context and for subsamples
484 from the same sherd. This variability may not be especially problematic for age
485 determinations made by current methods where diffusion coefficients are empirically
486 determined for each sample at the estimated archaeological temperature (Wilson et al.
487 2009, 2012).

488 Several different processes are occurring during rehydroxylation of clays with
489 differing structural properties. As proposed by Clegg et al. (2012), the surface layer of
490 water is a sufficient reservoir for the formation of hydroxyls that supply the single-order
491 diffusion process within narrow channels of the meta-clay (Ince et al. 2014).
492 Experiments by Mesbah et al. (2010a) clearly show that as the firing temperature
493 increases between 700-1200°C for kaolinite that the rate of fractional mass gain during
494 Stage II water absorption declines between 800-1200°C, with the most significant decline
495 at 900°C, as the clay is hardened, declines in porosity, and becomes increasingly dense
496 (Baccour et al. 2009). At the higher temperatures (1200°C) the amorphous silica, or
497 metakaolinite, is converted to cristobalite and the reactivity of the kaolinite to moisture is
498 decreased. This is also reflected in the reduction of clay surface area which limits the
499 reactivity with moisture (Mesbah 2010b).

500 At lower temperatures (600-900°C), amorphous silica, or meta-clays, dominate
501 but some amount of intact crystalline structure may be present. We interpret the
502 declining activation energies to reflect the change from reversible DHX to non-reversible
503 DHX (Shoval 1991), except for kaolinite which is non-reversible at temperatures below
504 600°C. At the very lowest temperatures, some of the fundamental structure is still present
505 and RHX may be able to reconstitute the original mineral structure. As temperatures rise,
506 the conversion to amorphous meta-clays increases and creates a strongly absorbing and
507 highly active surface (Shoval and Paz 2013) that contains the restricted diffusion
508 pathways. Even though there may be less available total moisture there are many more
509 diffusion sites as the structure changes and meta-clays increase in concentration. This is
510 accompanied by a lowering of the activation energy as the number of reaction sites
511 increases. We can anticipate that activation energy values will later rise as the meta-clay
512 is converted to spinel, mullite and other crystalline phases at temperatures in excess of
513 1000°C.

514 Additional work is also needed to more fully quantify the relationship between
515 activation energies and firing temperature that have been started here. As the ceramic
516 RHX dating method progresses, two situations can be anticipated where where a
517 knowledge of the activation energy value is critical. The first is when an improved
518 lifetime temperature estimate requires a recalculation of the previous age determination
519 (Clelland et al. 2015; Hall et al. 2013). Second, if abbreviated OH gain procedures are
520 eventually developed and empirically developed diffusion coefficients are to be
521 extrapolated to other samples in an assemblage, it will be necessary to estimate an
522 activation energy value appropriate to the degree of structural collapse for a particular

523 clay composition. The infrared spectroscopic method developed here is a beginning step
524 to address these potential needs and the understanding of the many variables impacting
525 the RHX process.

526 **7.0 Conclusion**

527

528 The rehydroxylation dating of ceramic materials holds great potential for
529 archaeological studies and initial results have been encouraging. A number of
530 complicating issues are likely to emerge in refinement of the method and one potential
531 problem is the occurrence of low-fired earthenware ceramics where the clay crystalline
532 structure has not fully transformed into an amorphous matrix. Under such circumstances
533 a range of activation energies may contribute to structuring the rehydroxylation process.
534 It is recommended that the firing temperature of a ceramic be established by infrared
535 analysis of the Si-O peak position to better understand the role of clay structural
536 transformations and their impact on the RHX process.

537

538 **Acknowledgments**

539

540 We would like to thank Richard Bland College for facility support and Everett Carpenter
541 of Virginia Commonwealth University for the X-ray diffraction analysis. Rachael Cagias
542 kindly provided the clay samples from St. Catherine's Island, Georgia, and David Hurst
543 Thomas provided the prehistoric ceramics. This research was funded by the National
544 Science Foundation (Award 1141218).

545

546 **References Cited**

547 .

548 Bala, P., Samantary, B.K., Srivastava, S.K. 2000. Dehydration transformation in Ca-
549 montmorillonite. *Bulletin of Material Science* 23, 1, 61-67.

550

551 Barrett, G.T. 2013. Rehydroxylation dating of fired clays: an improved time-offset model
552 to account for the effect of cooling on post-reheating mass gain. *Journal of*
553 *Archaeological Science* 40, 10, 3596-3603.

554

555 Bellotto, M., Gualtieri, A.F., Artioli, G., Clark, S.M. 1995. Kinetic study of the kaolinite-
556 mullite reaction sequence. I. Kaolinite dehydration. *Physics and Chemistry of Minerals*
557 22, 207-214.

558

559 Benedetto, de G.E., Laviano, R., Sabbatini, L., Zambonin, P.G. 2002. Infrared
560 spectroscopy in the mineral characterization of ancient pottery. *Journal of Cultural*
561 *Heritage* 3, 177-186.

562

563 Biljana, R. I., Mitrović, A.A., Miličić, L.R. 2010. Thermal treatment of kaolin clay to obtain
564 metakaolinite. *Hemisjka Industrija* 64, 4, 351-356

565

566 Bish, D.L. 2010. Rietveld refinement of the kaolinite structure at 1.5K. *Clay and Clay*
567 *Minerals* 41, 738-744.

568

569 Bowen, P.K., Ranck, H.J., Scarlett, T.J., Drelich, J.W. 2011.
570 Rehydration/rehydroxylation kinetics of reheated XIX-century Davenport (Utah)
571 ceramic. *Journal of the American Ceramic Society* 94, 2585-2591.
572

573 Bowen, P., Drelich, J., Scarlett, T.J. 2013. Modeling rehydration/rehydroxylation mass-
574 gain curves from Davenport ceramics. *Journal of the American Ceramic Society* 96, 3,
575 885-891.
576

577 Bradley, W.F., Grim, R.E. 1951. High temperature thermal effects of clay and related
578 materials. *American Mineralogist* 36, 182-201.
579

580 Clegg, F., Breen, C., Carter, M.A., Ince, C., Savage, S.D., Wilson, M.A. 2012.
581 Dehydroxylation and rehydroxylation mechanisms in fired clay ceramic: A TG-MS and
582 DRIFTS investigation. *Journal of the American Ceramic Society* 95, 1, 416-422.
583

584 Clelland, S.-J., Wilson, M.A., Carter, M.A., Batt, C.M. 2014. RHX dating: Measurement
585 of the activation energy of rehydroxylation for fired-clay ceramics. *Archaeometry* 57, 2,
586 392-404.
587

588 Cloutis, E.A. 2001. Analytical Data for Mineral and Rock Samples. Mount Holyoke
589 College, South Hadley, MA.

590 Criado, J.M., Ortega, A., Real, C., Torres de Torres, E. 1984. Re-examination of the
591 kinetics of dihydroxylation of kaolinite. *Clay Minerals* 19, 653-661.

592 Cultrone, G., Rodriguez-Navarro, C., Sebastian, E., Cazalla, O., and De La Torre, M.J.
593 2001. Carbonate and silica phase reactions during ceramic firing. *European Journal of*
594 *Mineralogy* 13, 621-634.

595

596 Drebuschak, V.A., Mylnikova, L.N., Modolin, V.I. 2007. Thermogravimetric
597 investigation of ancient ceramics. *Journal of Thermal Analysis and Calorimetry* 90:73-
598 79.

599

600 Drelich, J., Bowen, P.K., Scarlett, T.J. 2013. Effect of humidity instability on
601 rehydroxylation in fired clay ceramics. *Journal of the American Ceramic Society* 96, 4,
602 1047-1050.

603

604 Drits, V.A., McCarthy, D.K. 2007. The nature of structure-bonded H₂O in illite and
605 leucophyllite from dehydration and dehydroxylation experiments. *Clays and Clay*
606 *Minerals* 55, 45-58.

607

608 Drits, V.A., Besson, G., Muller, F. 1995. An improved model for structural
609 transformations of heat-treated aluminous dioctahedral 2:1 layer silicates. *Clays and Clay*
610 *Minerals* 43, 718-731.

611

612 Drits, V.A., Zviagina, B.B., McCarthy, D.K., Salyn, A.L. 2010. Factors responsible for
613 crystal-chemical variations in the solid solutions from illite to aluminoceladonite and
614 from glauconite to celadonite. *American Mineralogist* 95, 348-361.

615

616 Felicissimo, M.P., Peixoto, J.L., Bittencourt, C., Tomasi, R., Houssiau, L., Pireaux, J-J.,
617 Rodrigues-Filho, U.P. 2010. SEM, EPR, and ToF-SIMS analyses applied to unravel the
618 technology employed for pottery-making by pre-colonial Indian tribes from Pantanal,
619 Brazil. *Journal of Archaeological Science* 37, 9, 2179-2187.

620

621 Ferrage, E., Tournassat, C., Rinnert, E., Lanson, B. 2005. Influence of pH on the
622 interlayer cationic composition and hydration state of Ca-montmorillonite: Analytical
623 chemistry, chemical modelling and XRD profile modelling study. *Geochimica et*
624 *Cosmochimica Acta* 69, 11, 2797–2812

625

626 Forney, C.F., Brandl, D.G. 1992. Control of humidity in small controlled environment
627 chambers using glycerol-water solutions. *Horticultural Technology* 2, 1, 52-54.

628

629 Frost, R.L., Vassallo, A.M. 1996. The dehydroxylation of the kaolinite clay minerals
630 using infrared emission spectroscopy. *Clay and Clay Minerals* 44, 635-651.

631

632 Frost, R.L.; Horvath, E.; Mako, E.; Kristof, J., Redey, A. 2003. Slow transformation of
633 mechanically dehydroxylated kaolinite to kaolinite - an aged mechanochemically
634 activated formamide - intercalated kaolinite study. *Thermochimica Acta*. 408, 1-2, 103-
635 113.

636

637 Gosselain, O.P. 1992. Bonfire in the inquiries. Pottery firing temperatures in archaeology:
638 What for? *Journal of Archaeological Science* 19, 3, 243-259.
639
640 Grim, R.E., Bradley, W.F. 1948. Rehydration and dehydration of the clay minerals.
641 *American Mineralogist* 33, 50-59.
642
643 Gualtieri, A.F., Ferrari, S. 2006. Kinetics of illite dehydroxylation. *Physics and*
644 *Chemistry of Minerals* 33:490-501.
645
646 Hall, C., Hamilton, A., Wilson, M.A. 2013. The influence of temperature on
647 rehydroxylation [RHX] kinetics in archaeological pottery. *Journal of Archaeological*
648 *Science* 40, 305-312.
649
650 Hamilton, A., Hall, C. 2012. A review of rehydroxylation in fired-clay ceramics. *Journal*
651 *of the American Ceramic Society* 95, 9, 2673-2678.
652
653 Ince, C., Derogar, S. 2014. Mass gain in fired clay ceramics. *Journal of the Australian*
654 *Ceramics Society* 50, 2, 59-67.
655
656 Krapukaityte, A., Tautkus, S., Kareiva, A., Zalieckiene, E. 2008. Thermal analysis- a
657 powerful tool for the characterization of pottery. *CHEMIJA* 19, 2, 4-8.
658

659 Le Goff, M., Gallet, Y. 2014. Evaluation of the rehydroxylation dating method: Insights
660 from a new measurement device. *Quaternary Geochronology* 20, 89-98.
661

662 Le Goff, M., Gallet, Y. 2015. Experimental variability in kinetics of **moisture** expansion
663 and mass gain in ceramics. *Journal of the American Ceramic Society* 98, 2, 398-401.
664

665 Madejova, J., Komadel, P. 2001. Baseline Studies of the Clay Minerals Society Source-
666 Clays: Infrared Methods. *Clays and Clay Minerals* 49, 5, 410–432.
667

668 Maggetti, M., Neururer, Ch., Ramseyer, D. 2011. Temperature evolution inside a pot
669 during experimental (bonfire) firing. *Applied Clay Science* 53, 500-508.
670

671 Marghussian, A.K., Fazeli, H., Sarpoolaky, H. 2009. Chemical-mineralogical analyses
672 and microstructural studies of prehistoric pottery from Rahmatabad, South-west Iran.
673 *Archaeometry* 51, 5, 733-747.
674

675 McConville, C.J., Lee, W.E. 2005. Microstructural development on firing illite and
676 smectite clays compared with that in kaolinite. *Journal of the American Ceramic Society*
677 88, 8, 2267-2276.
678

679 Mermut, A.R., Cano, A.F. 2001. Baseline studies of the Clay Minerals Society source
680 clays: chemical analysis of major elements. *Clay and Clay Minerals* 49, 5, 381-386.
681

682 Mesbah, H., Wilson, M.A., Carter, M.A. 2010a. The role of kaolinite-mullite reaction
683 sequence in moisture mass gain in fired kaolin. In proceedings of the 12th International
684 Ceramics Congress (CIMTEC 2010), Florence, Italy, 2010. eScholarID:145789.
685

686 Mesbah, H., Wilson, M.A., Carter, M.A. Shackleton, J. 2010b. Effect of prolonged
687 sintering time at 1200°C on the phase transformation and reactivity with moisture of fired
688 kaolinite. 11th International Conference on Ceramic Processing Science.
689 eScholarID:145792.
690

691 Mirti, P., Davit, P. 2001. Technological characterization of Campian pottery of type a, b,
692 and c and of regional products from ancient Calabria (southern Italy). *Archaeometry* 1,
693 19-33.
694

695 Mirti, P., Perardi, A., Gulmini, M. 2006. A scientific investigation of the provenance and
696 technology of a black-figure amphora attributed to the Priam Group. *Archaeometry* 48,
697 31-43.
698

699 Muller, F., Pons, C.H., Papin, A. 2002. Study of dehydroxylated-rehydroxylated
700 smectites by SAXS. *Journal of Physics IV France* 12.
701

702 Numrich, M, Kutschera, W., Steier, P., Sterba, J.H., Golser, R. 2015. On the effect of
703 organic carbon on rehydroxylation (RHX) dating. *Journal of Archaeological Science* 57,
704 92-97.

705

706 Odriozola, C., Martinez-Blanes, J.M. 2007. Estimate of firing temperatures through
707 bone-based Chalcolithic decorated pottery. *Journal of Thermal Analysis and Calorimetry*
708 87, 1, 135-141.

709

710 Ogloza, A.A., Malhotra, V.M. 1989. Dehydroxylation induced structural transformations
711 in montmorillonite: an isothermal FTIR study. *Physics and Chemistry of Minerals* 16,
712 378-385.

713

714 Ortega, A., Macias, M., Gotor, F.J. 2010. The multistep nature of kaolin
715 dehydroxylation; kinetics and mechanism. *Journal of the American Ceramic Society* 93,
716 197-203.

717

718 Palanivel, R., Rajesh Kumar, U. 2011. The mineralogical and morphological studies on
719 archaeological pottery shreds. *Recent Research in Science and Technology* 1, 3, 109-115.

720

721 Papadopoulou, D.N., Lalia-Kantouri, M., Kantiranis, N., Stratis, J.A. 2006. Thermal and
722 mineralogical contribution to the ancient ceramics and natural clays characterization.
723 *Journal of Thermal Analysis and Calorimetry* 84, 39-45.

724

725 Pesova, A. Andertova, J., Gedeon, O. 2010. Hydrothermal degradation of ceramic
726 materials on the natural raw materials base. Part 2: structural changes. *Ceramics-Silikaty*
727 54, 176-181.

728

729 Ravisankar, R., Kiruba, S., Chandrasekaran, A., Naseerutheen, A., Seran, M., Balaji, P.D.
730 2010. Determination of firing temperature of some ancient potteries of Tamil Nadu,
731 India by FT-IR spectroscopic technique. *Indian Journal of Science and Technology* 3, 9,
732 1016-1019.

733

734 Rodriguez-Navarro, C., Ruiz-Agudo, E., Luque, A., Rodriguez-Navarro, A.B., Ortega-
735 Huertas, M. 2009. Thermal decomposition of calcite: Mechanisms of formation and
736 textural evolution of CaO nanocrystals. *American Mineralogist* 94, 578-584 .

737

738 Sand, C., Valentin, F., Sorovi-Vunidilo, T. 2000. At the borders of Polynesia:
739 archaeological research in the East-Fijian islands of Cikoba and Naquelevu. *Indo-Pacific*
740 *Prehistory Association Bulletin* 20. 4, 107-116.

741

742 Sato, T., Watanabe, T., Otsuka, R. 1992. Effect of layer charge, charge location, and
743 energy change on expansion properties of dioctahedral montmorillonites. *Clays and Clay*
744 *Minerals* 40, 103-113.

745

746 Savage, S.D., Wilson, M.A., Carter, M.A., Hoff, W.D., Hall, C., McKay, B. 2008.
747 Moisture expansion and mass gain in fired clay ceramics: A two-stage (time)^{1/4} process.
748 *Journal of Physics D: Applied Physics* 41, 5, 055402.

749

750 Shepard, A.O. 1976. *Ceramics for the Archaeologist*. Carnegie Institute of Washington,
751 Publication 609, Washington, D.C., 5th Edition.
752

753 Shoval, S. 2003. Using FT-IR spectroscopy for the study of calcareous ancient ceramics.
754 *Optical Materials* 24, 117-122.
755

756 Shoval, S., Beck, P. 2005. Thermo-FTIR spectroscopy analysis as a method of
757 characterizing ancient ceramic technology. *Journal of Thermal Analysis and Calorimetry*
758 82, 609-616.
759

760 Shoval, S., Beck, P., Kirsh, D., Levy, D., Gaft, M., Yadin, E. 1991. Rehydroxylation of
761 clay minerals and hydration in ancient pottery from the 'Land of Geshur'. *Journal of*
762 *Thermal Analysis* 37, 1579-1592.
763

764 Shoval, S., Yadin, E., Panczer, G. 2011. Analysis of thermal phases in calcareous Iron
765 Age pottery using FT-IR and Raman spectroscopy. *Journal of Thermal Analysis and*
766 *Calorimetry* 104, 515-525.
767

768 Shoval, S., Paz, Y. 2013. A study of the mass-gain of ancient pottery in relation to
769 archaeological ages using thermal analysis. *Applied Clay Science* 82, 113-120.
770

771 Smith, A. L. 2001. Bonfire II: The return of pottery firing temperatures. *Journal of*
772 *Archaeological Science* 28, 9, 991-1003.

773

774 Smith, K., Neiman, F. 2007. Frequency seriation, correspondence analysis, and
775 Woodland Period ceramic assemblage variation in the Deep South. *Southeastern*
776 *Archaeology* 26, 1, 47-72.

777

778 Sperinck, S., Raiteri, P., Marks, N., Wright, K. (2011). Dehydroxylation of kaolinite to
779 metakaolin- a molecular dynamics study. *Journal of Materials Chemistry* 21, 2118-2125.

780

781 Tite, M.S. 1999. Pottery production, distribution and consumption—The contribution of
782 the physical sciences. *Journal of Archaeological Method and Theory* 6, 3, 181-233.

783

784 Tosheva, L., Mihailova, B., Wilson, M.A., Carter, M.A. 2010. Gravimetric and
785 spectroscopic studies of the chemical combination of moisture by as-fired and reheated
786 terracotta. *Journal of the European Ceramic Society* 30, 1867-1872.

787

788 Trindade, M.J., Dias, M.I., Coroado, J., Rocha, F. 2009. Mineralogical transformations of
789 calcareous rich clays with firing: A comparative study between calcite and dolomite rich
790 clays from Algarve, Portugal. *Applied Clay Science* 42, 345-255.

791

792 Tsipursky, S.I., Drits,, V.A. 1984. The distribution of octahedral cations in the 2:1 layers
793 of dioctahedral smectites studied by oblique-texture electron diffraction. *Clay Minerals*
794 19, 177-193.

795

796 Venkatachalapathy, R., Bakas, T., Basavaiah, N., Deenadayalan, K. 2008. Mossbauer
797 and mineral magnetic studies on archaeological potteries from Adhichanallur, Tamilnadu,
798 India. *Hyperfine Interact* 186, 89-98.
799

800 Venkatachalapathy, R., Sridharan, T., Dhanapandian, S., Manoharan, C. 2002.
801 Determination of firing temperature of ancient potteries by means of infrared and
802 Mossbauer studies. *Spectroscopy Letters* 35, 769-779.
803

804 Viani, A. Gualtieri, A.F., Artioli, G. 2002. The nature of disorder in montmorillonite by
805 simulation of X-ray powder patterns. *American Mineralogist* 87, 966-975.
806

807 Wagner, U., Gebhard, R., Hausler, W., Hutzelmann, T., Riederer, J., Shimada, I., Sosa, J.,
808 Wagner, F.E., 1999. Reducing firing of an early pottery making kiln at Batan Grande,
809 Peru: a Mossbauer study. *Hyperfine Interactions* 122, 163-170.
810

811 Wilson, M.A., Carter, M.A., Hall, C., Hoff, W.D., Ince, C., Savage, S.D., McKay, B.,
812 Betts, I.M. 2009. Dating fired-clay ceramics using long-term power law rehydroxylation
813 kinetics. *Proceedings of the Royal Society A*. A 465, 2407-2415.
814

815 Wilson, M.A., Hamilton, A., Ince, C., Carter, M.A., Hall, C. 2012. Rehydroxylation
816 (RHX) dating of archaeological pottery. *Proceedings of the Royal Society A* 468 2147,
817 3476-3493.
818

819 Wilson, M.A., Clelland, S., Carter, M.A., Ince, C., Hall, C., Hamilton, A., Batt, C.M.
820 2014. Rehydroxylation of fired clay ceramics: Factors effecting early mass gain in dating
821 experiments. *Archaeometry* 56, 4, 689-702.
822

823 Wolf, S. 2002. Estimation of the production parameters of very large medieval bricks
824 from St. Urban, Switzerland. *Archaeometry* 44, 37-65.
825

826 Yates, D.M., Rosenburg, P.E. 1997. Formation and stability of endmember illite: II.
827 Solid equilibration experiments at 100 to 250°C and P_{CO₂}. *Geochimica et Cosmochimica*
828 *Acta* 61, 3135–3144.
829

830 Zemenova, P., Klouzkova, A., Kohoutkova, M., Kral, R. 2014. Investigation of the first
831 and second dehydroxylation of Kaolinite. *Journal of Thermal and Analytical Calorimetry*
832 116:633-639.
833

834 **List of Tables**

835

836 Table 1. Infrared peak positions for kaolinite (KGa-2), montmorillonite (Stx-1b), and
837 illite heated to 600-1000°C for 24 hours.

838

839 Table 2. Infrared peak positions at different temperatures for St. Catherine's Island clays
840 (SCI-RC-1, SCI-RC-2, and SCI-RC-4).

841

842 Table 3. Infrared peak positions for Saint Catherine's Island archaeological ceramics.

843

844 Table 4. Rehydroxylation slope values between 110-150°C used for the activation energy
845 determinations of kaolinite, illite, and montmorillonite.

846

847 Table 5. Activation energies (J/mol) for kaolinite, illite, and montmorillonite between
848 600-900°C.

849

850 **List of Figures**

851

852 Figure 1. Map of St. Catherine's Island, Georgia, showing the location of the three clay
853 sources and the archaeological sites mentioned in the text.

854

855 Figure 2. Plots of infrared Si-O peak position locations (cm^{-1}) for (A) kaolinite (KGa-2),
856 (B) montmorillonite (Stx-1b), and (C) illite.

857

858 Figure 3. Superimposed infrared spectra showing the position of the Si-O peaks at
859 300°C, 800°C, and 1000°C for clay SCI-RC-1.

860

861 Figure 4. Infrared spectra of St. Catherine's Island clays (SCI-RC-1, SCI-RC-2, SCI-RC-
862 4) at 500-1000°C showing the abrupt shift in the Si-O peak ($\sim 1030\text{cm}^{-1}$) to higher
863 wavenumbers with increasing temperature. Triangle=SCI-RC-1, Circle=SCI-RC-2,
864 Square=SCI-RC-4.

865

866 Figure 5. Infrared peak locations from the interior (1) to exterior (5) of Sherd 4079
867 showing the peak position changes.

868

869 Figure 6. Representative plot of kaolinite rehydroxylated at 120°C after dehydroxylation
870 at 700°C.

Table 1. Infrared peak positions for kaolinite (KGa-2), montmorillonite (Stx-1b), and illite heated to 600-1000°C for 24 hours. Peak position resolution is 4cm⁻¹.

Firing		
Temperature (°C)	Peak Position (cm⁻¹)	Peak Position (cm⁻¹)
<i>KGa-2</i>	Amorphous Si	Si-O Stretch
600	1216	1075
700	1225	1081
800	1227	1086
900	1237	1096
1000	1242	1100
<i>STx-1b</i>	Si-O Stretch	Si-O-Si Deformation
600	1041	480
700	1043	483
800	1090	483
900	1094	475
1000	1093	474
<i>Illite</i>	Si-O Stretch	Si-O-Si Bend
600	1012	482
700	1006	481
800	1013	482
900	1078	463
1000	1081	463

Table 2. Infrared peak positions at different temperatures for St. Catherine's Island clays (SCI-RC-1, SCI-RC-2, and SCI-RC-4). Peak position resolution is 4cm^{-1} . Peak position resolution is 4cm^{-1} .

Temperature (°C)	Time (hours)	Peak Position (cm^{-1})
<i>SCI-RC-1</i>		
		Si-O Stretch
500	24	1037
600	24	1034
700	24	1034
800	4	1034
900	3	1089
1000	4	1089
<i>SCI-RC-2</i>		
		Si-O Stretch
500	24	1037
600	24	1031
700	24	1033
800	4	1035
900	3	1095
1000	4	1090
<i>SCI-RC-4</i>		
		Si-O Stretch
500	24	1034
600	24	1032
700	24	1033
800	4	1034
900	3	1095
1000	4	1087

Table 3. Infrared peak positions for Saint Catherine's Island archaeological ceramics. Peak position resolution is 4cm^{-1} .

Ceramic Sherd	Sample Location	Peak Position (cm^{-1})	Estimated Firing Temperature ($^{\circ}\text{C}$)
<i>Site 9Li207</i>		Si-O Stretch	
4079	1: Interior surface	1034	<900
4079	2: Interior	1052	<900
4079	3: Interior	1054	<900
4079	4: Interior	1048	<900
4079	5 Exterior surface	1042	<900
<i>Site 9Li8</i>			
29347	Feature 45	1039	<900
29672	Feature 68	1046	<900
30467	Feature 9	1083	<900
32011	Feature 11	1066	<900
36523	Feature 98	1051	<900

Table 4. Rehydroxylation slope values between 110-150°C used for the activation energy determinations of kaolinite, illite, and montmorillonite.

Kaolinite (KGa-2)				
Experiment	RHX Temp (°C)	Slope	1/Kelvin	Ln Slope
DHX 600°C				
NSF-46	150	0.0506	2.3632	-2.984
NSF-46	140	0.0423	2.4204	-3.163
NSF-46	130	0.0338	2.4804	-3.387
NSF-46	120	0.0299	2.5435	-3.510
NSF-46	110	0.0200	2.6099	-3.912
DHX 700°C				
NSF-12	150	0.0379	2.36	-3.273
NSF-13	140	0.0360	2.42	-3.324
NSF-15	130	0.0271	2.48	-3.608
NSF-16	120	0.0259	2.54	-3.654
NSF-17	110	0.0188	2.61	-3.974
DHX 800°C				
NSF-18	150	0.0853	2.3632	-2.462
NSF-34R	140	0.0907	2.4204	-2.400
NSF-20	130	0.0784	2.4804	-2.546
NSF-22	120	0.0615	2.5435	-2.789
NSF-24	110	0.0512	2.6099	-2.972
DHX 900°C				
NSF-25	150	0.0968	2.3632	-2.335
NSF-26	140	0.1112	2.4204	-2.196
NSF-28	130	0.0991	2.4804	-2.312
NSF-29	120	0.0886	2.5435	-2.424
NSF-48	110	0.0764	2.6099	-2.572
Illite				
Experiment	RHX Temp (°C)	Slope	1/T*1000	Ln Slope
DHX 700°C				
NSF-103	150	0.0325	2.3632	-3.4265
NSF-107	140	0.0283	2.4204	-3.5649
NSF-109	130	0.0284	2.4805	-3.5614

NSF-127	120	0.0178	2.5436	-4.0286
NSF-116	110	0.0152	2.6099	-4.1865
Experiment	RHX Temp (°C)	Slope	1/T*1000	Ln Slope
DHX 900°C				
NSF-104	150	0.0599	2.3632	-2.8151
NSF-106	140	0.0569	2.4204	-2.8665
NSF-108	130	0.0500	2.4805	-2.9957
NSF-113	120	0.0469	2.5436	-3.0597
NSF-123	110	0.0426	2.6099	-3.1559
Montmorillonite (Stx-1b)				
Experiment	RHX Temp (°C)	Slope	1/T*1000	Ln Slope
DHX 700°C				
NSF-180	150	0.0840	2.3632	-2.4769
NSF-181	140	0.0680	2.4204	-2.6882
NSF-199	130	0.0585	2.4805	-2.8387
NSF-195	120	0.0403	2.5436	-3.2114
NSF-194	110	0.0357	2.6099	-3.3326
Experiment	RHX Temp (°C)	Slope	1/T*1000	Ln Slope
DHX 900°C				
NSF-174	150	0.1065	2.3632	-2.2396
NSF-204	140	0.0883	2.4204	-2.4270
NSF-173	130	0.0762	2.4805	-2.5744
NSF-179	120	0.0604	2.5436	-2.8068
NSF-166	110	0.0528	2.6099	-2.9412

Table 5. Activation energies (J/mol) for kaolinite, illite, and montmorillonite between 600-900°C.

Temperature (°C)	Kaolinite (KGa-2)	Illite	Montmorillonite (STx-1b)
600	119,218	--	--
700	93,718	107,571	120,468
800	76,731	--	--
900	65,242	47,181	96,059

Figure 1

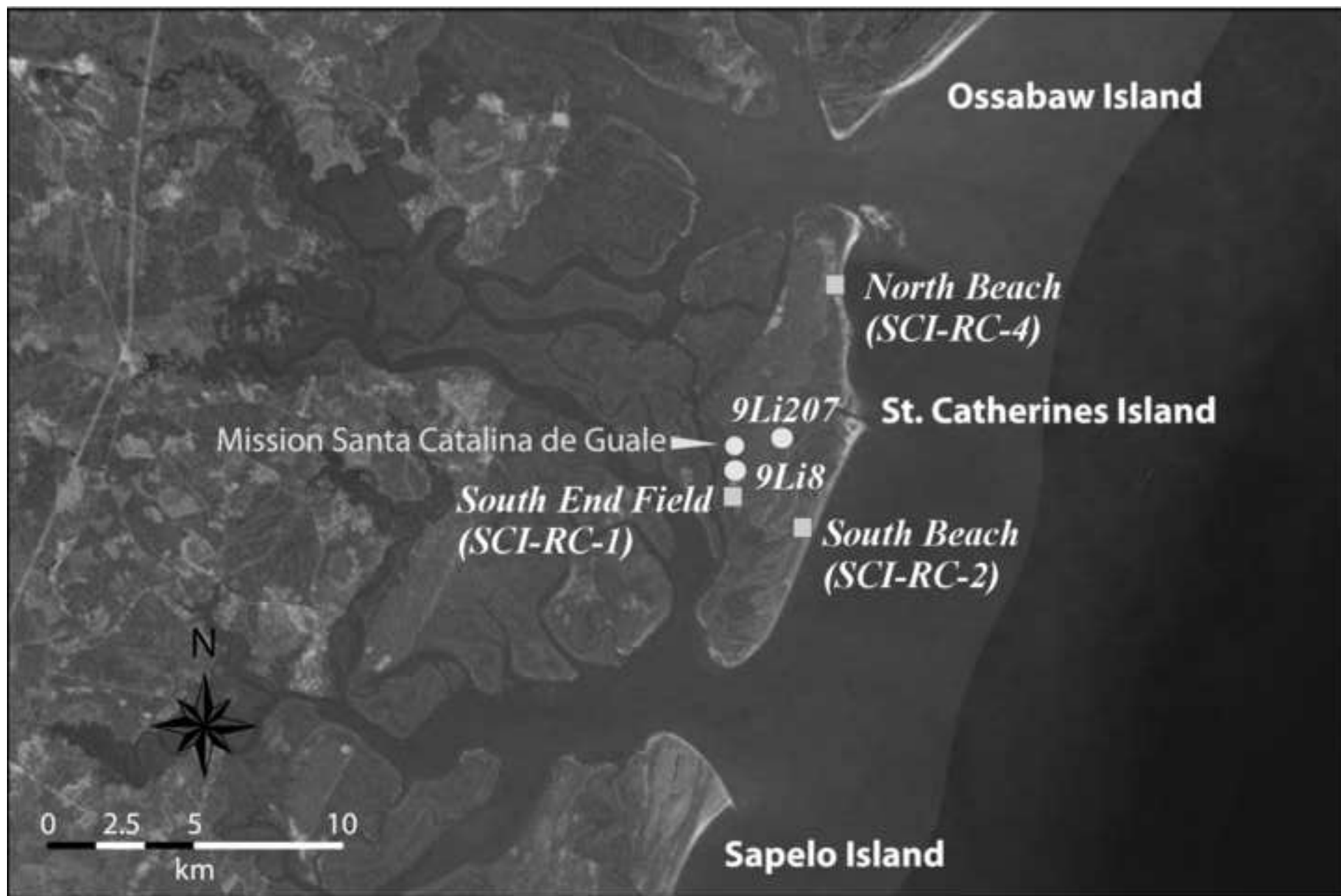


Figure 2

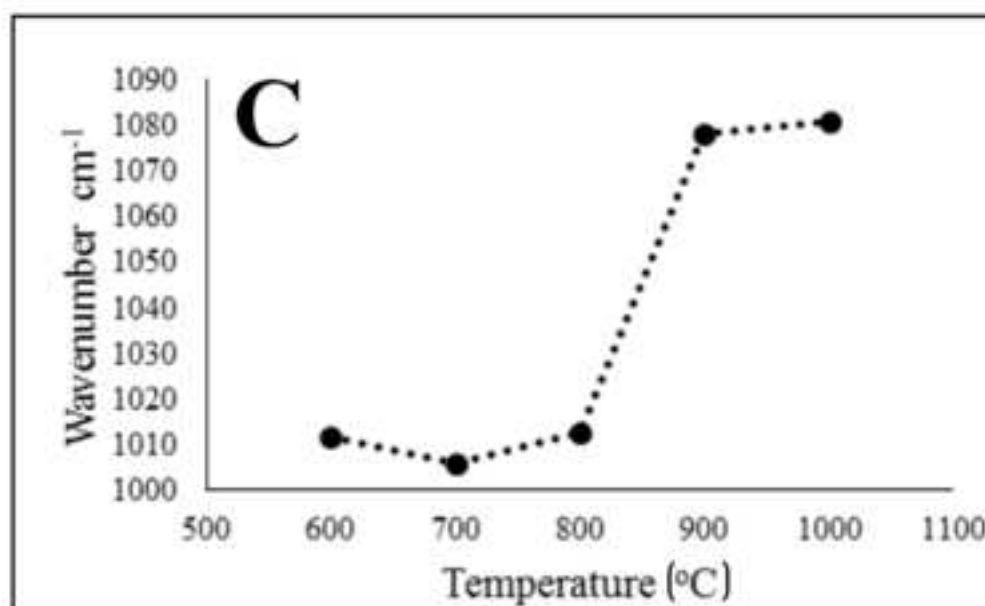
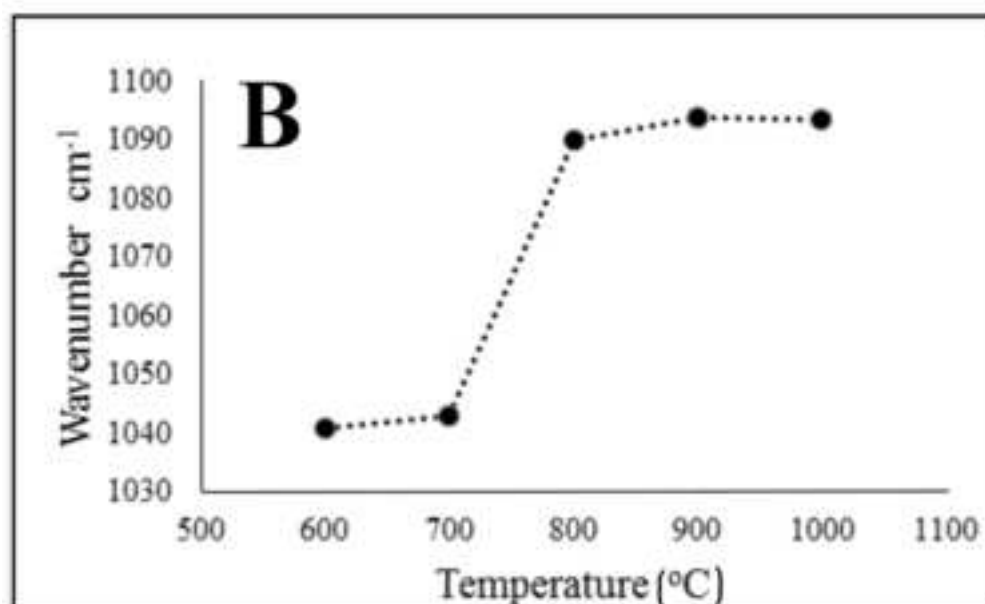
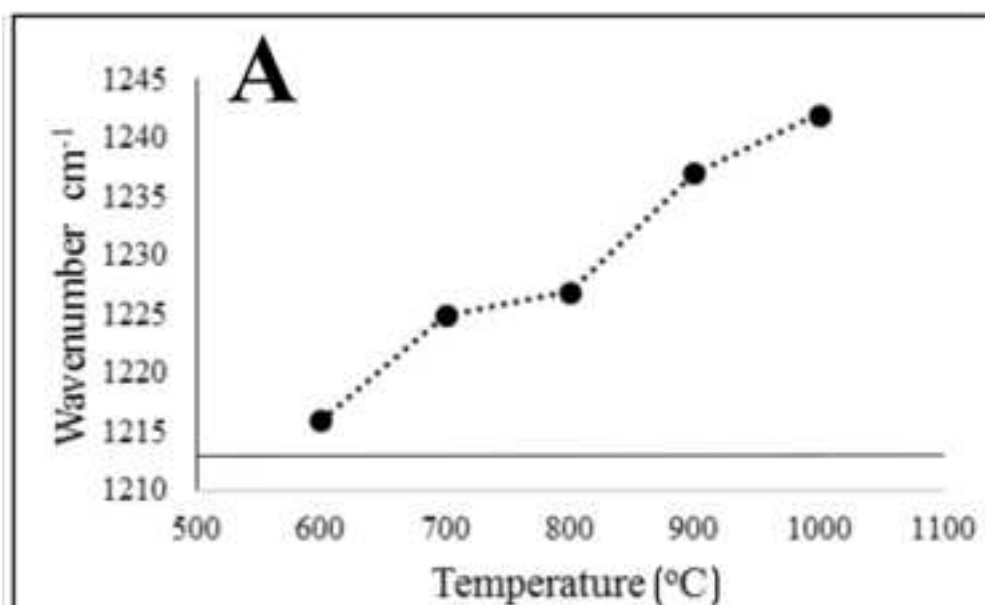


Figure 3

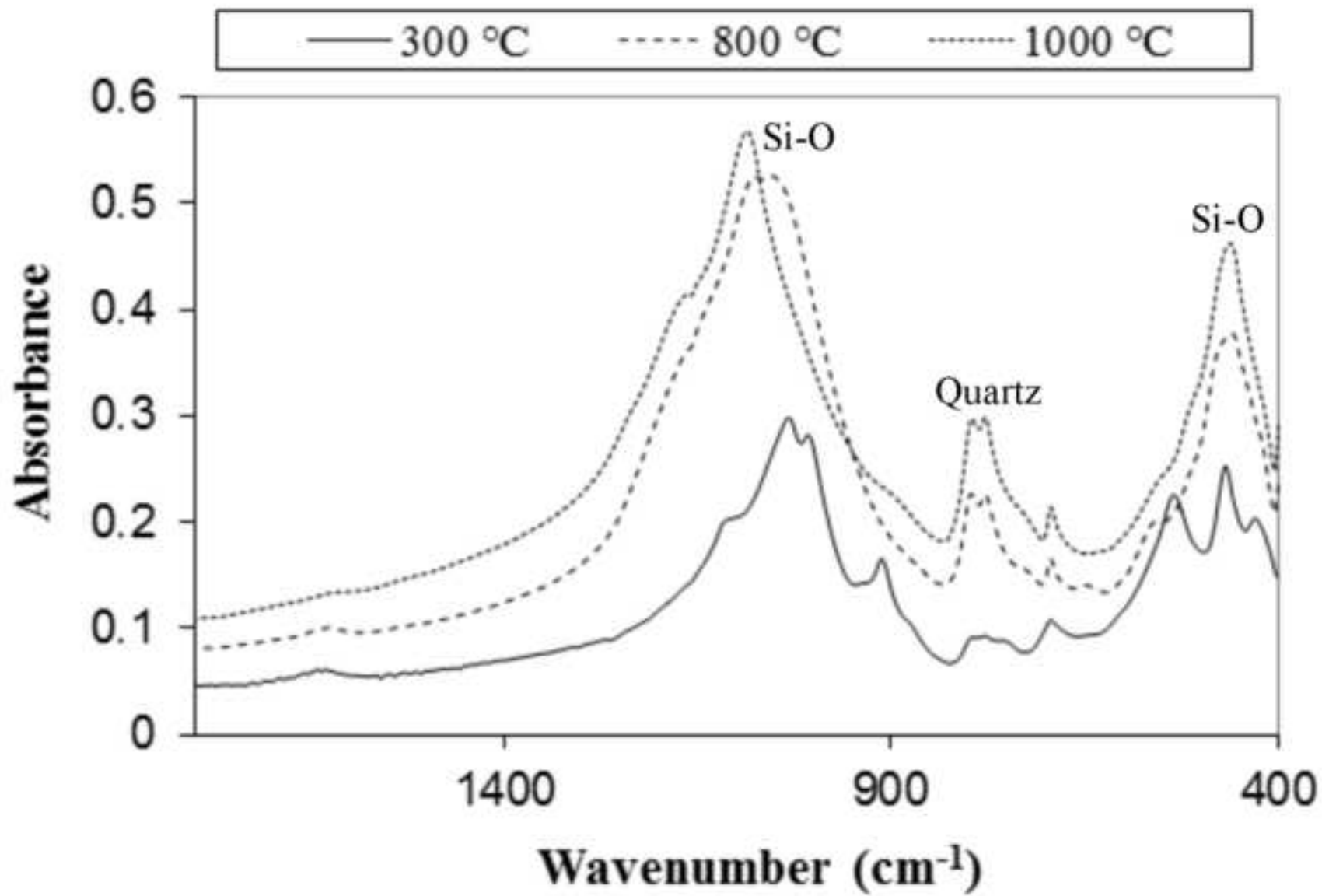


Figure 4

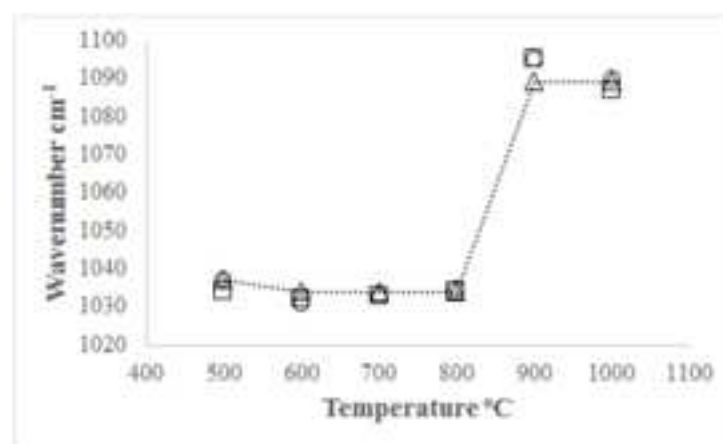


Figure 5

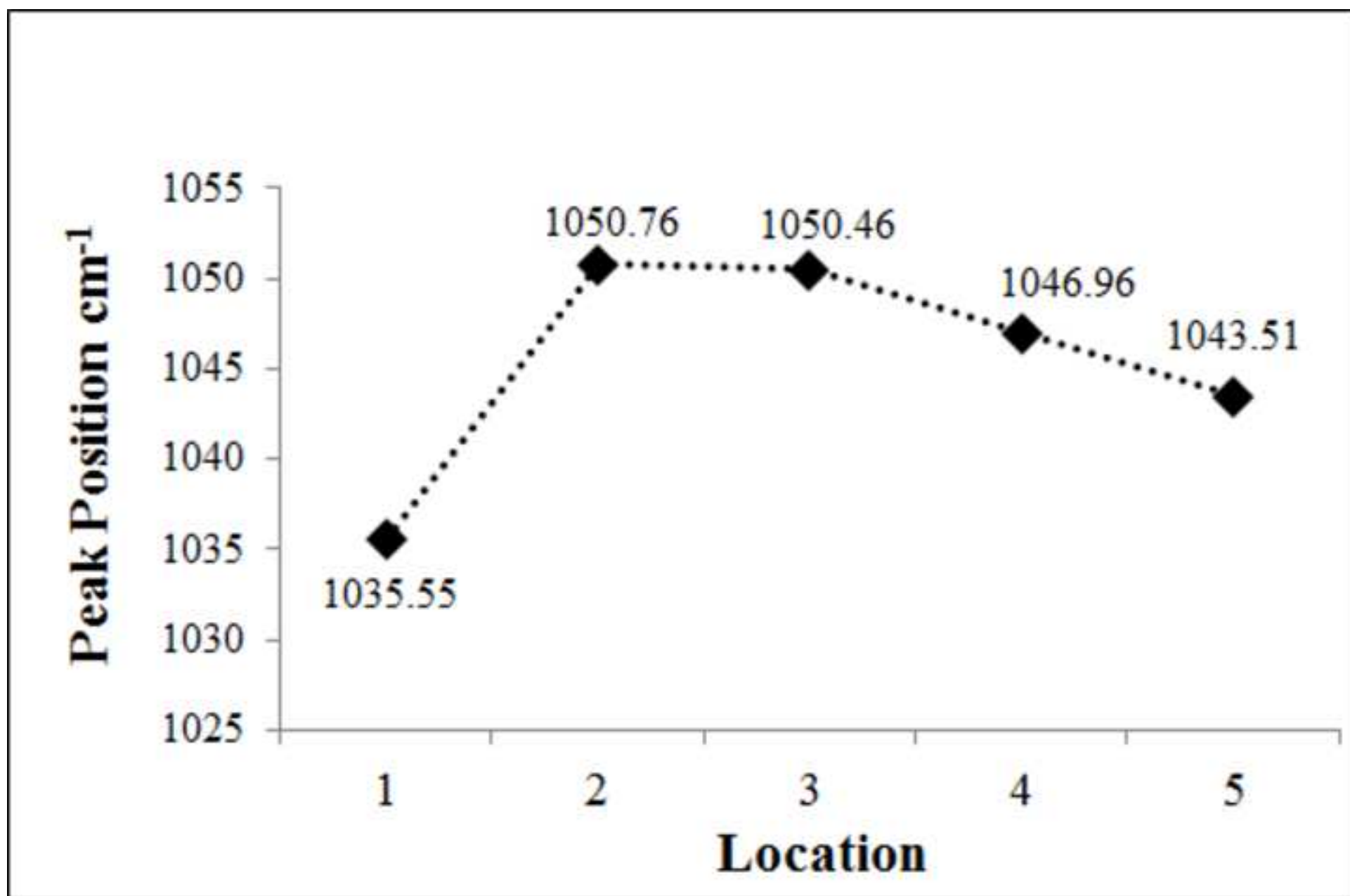


Figure 6

